Dispersed fluorescence spectroscopy of AlNi, NiAu, and PtCu

Jacqueline C. Fabbi
Department of Chemistry, University of Utah, Salt Lake City, Utah 84112

Lars Karlsson
Department of Physics, Stockholm University, Vanadisvägen 9, 11346 Stockholm, Sweden

Jon D. Langenberg, Quinton D. Costello, and Michael D. Morse
Department of Chemistry, University of Utah, Salt Lake City, Utah 84112

(Received 4 February 2003; accepted 24 February 2003)

Dispersed fluorescence studies of AlNi, NiAu, and PtCu have been performed, providing spectroscopic information about the ground and low-lying excited electronic states. Vibrational frequencies are reported for the ground $X\,^2\Delta_{5/2}$ state of all three molecules. In the case of AlNi, fluorescence to all five of the states originating from the $3d^9_{\mathrm{Ni}}3s^2_{\mathrm{Al}}\sigma^2$ manifold has been observed. For both NiAu and PtCu, fluorescence to two low-lying excited states in addition to the ground state was observed. Relative energies, vibrational constants, and, when possible, Ω values of these states are reported. Comparisons of the measured electronic states to the predictions of a ligand-field plus spin–orbit model are also provided, along with a comparison of the electronic structure of PtCu to that of PtH. © *2003 American Institute of Physics.* [DOI: 10.1063/1.1567712]

I. INTRODUCTION

To gain a better understanding of the factors which govern the bonding in diatomic transition metals, systematic investigations of these species using the techniques of resonant two photon ionization (R2PI) and laser-induced fluorescence (LIF) spectroscopy of neutrals[1,2] and photodissociation spectroscopy of cations[3–5] have been pursued in this laboratory and elsewhere.[6–10] Much has also been learned through resonance Raman studies of mass-selected matrix isolated metal dimers[11] and photoelectron spectroscopy of mass-selected anions.[12–20] These techniques have provided considerable insight into the electronic structure of the diatomic transition metals, including ground and excited state symmetries and bond lengths, ground state bond energies, ionization energies, excited state lifetimes, excited state vibrational frequencies and anharmonicities, and in some cases vibrational intervals in the ground state.

In particular, the late transition metal dimers have been rather well studied.[2,15–18,21–27] In the coinage metals (Cu, Ag, Au), the d orbitals are both filled and highly contracted, such that when two $d^{10}s^1$ atoms combine the bonding is completely dominated by the s orbitals, which overlap to form a σ^2 bond in the $X\,^1\Sigma^+_{(g)}$ ground state. In the nickel group diatomics the open d orbitals greatly increase the number of low lying states and create the possibility of d orbital contributions to the bonding. As in the other open d subshell transition metals, the relative size of the d and s orbitals dictates the degree to which d orbital bonding may occur. Relativistic effects, for example, cause the $5d$ orbitals in platinum to be more available for bonding than the $3d$ orbitals in nickel. The possibility of d orbital contributions to the bonding in the nickel group and mixed nickel-coinage metal group dimers can be tested by comparing the bond energies and bond lengths of these diatomics to their coinage metal analogs. In cases where the d orbitals are greatly contracted and not participating in the chemical bonding, a ligand field treatment including spin–orbit effects has been developed.[28]

The ligand field model, as applied to diatomic transition metals, treats the molecule as two positively charged d^n cores surrounded by a diffuse σ^2 cloud.[28] In a molecule such as NiCu, the $3d^9_{\mathrm{Ni}}$ nickel core is perturbed by the positively charged copper $3d^{10}_{\mathrm{Cu}}$ core (the ligand), and the electrostatic perturbations of the $3d^9_{\mathrm{Ni}}$ core by the relatively diffuse and roughly spherical σ^2 cloud are neglected. The result is an energetic ordering of the $3d$ orbitals on the nickel atom as $3d\sigma < 3d\pi < 3d\delta$, with the most favorable placement of the $3d$ hole in the $3d\delta$ orbital. This results in an $X\,^2\Delta_{5/2}$ ground state for NiCu, as has been demonstrated experimentally.[29] Similarly, diatomic AlNi consists of an aluminum atom with a filled $3s$ orbital and a lone $3p$ electron, which bonds in a σ fashion with the $4s$ electron of a $3d^94s^1$ nickel atom, resulting in a $3d^9_{\mathrm{Ni}}3s^2_{\mathrm{Al}}\sigma^2$ manifold of states. Treating the aluminum atom as a $+1$ ligand, a $^2\Delta_{5/2}$ ground state is again predicted, and observed.[30] The ligand field model is also successful in predicting the ground states of NiAu,[31] PtCu,[31] NiH,[32,33] and PtH[34] (all $^2\Delta_{5/2}$), and Ni_2 (either 0^+_g or 0^-_u).[25]

Despite this success in correctly predicting the ground electronic state for a number of transition metal molecules, the ligand field model has not been seriously tested in its predictions of the energetic ordering of the remaining states arising from the ground manifold. The present dispersed fluorescence study was undertaken to provide experimental energies for the ground manifold of states in AlNi, NiAu, and PtCu for comparison to the ligand field model. These molecules were chosen for study instead of the prototypical molecule NiCu, because the known transitions in NiCu lie so far to the red that the detection range of the photomultiplier seriously limits the ability to look for low-lying excited states. In addition, the known transitions of NiCu occur in a wave number range where it is difficult to avoid simulta-

neously exciting Ni_2, which is of necessity present in any molecular beam containing NiCu. In addition, it was hoped that by studying PtCu, a molecule for which the ligand field model might be expected to be less applicable due to the greater availability of the $5d$ orbitals for bonding, additional insight might be gained.

II. LIGAND FIELD CALCULATIONS ON AlNi, NiAu, AND PtCu

In a previous paper on the application of ligand field theory to diatomic metals, Hund's case (a) basis functions and Hamiltonian matrices for the $d_A^9 d_B^{10}\sigma^2$ states of a heteronuclear transition metal molecule, such as NiAu or PtCu, were given.[28] These same basis functions and Hamiltonian matrices also apply to the $d_{Ni}^9 s_{Al}^2\sigma^2$ states of molecules such as AlNi. To apply the model to AlNi, NiAu, and PtCu, the only inputs required are the bond length of the molecule, R, the spin–orbit constant of Ni or Pt for the nd orbitals in the $nd^9(n+1)s^1$ configuration, ζ, and the expectation values of $\langle r^2\rangle_{nd}$ and $\langle r^4\rangle_{nd}$ for the $nd^9(n+1)s^1$ configuration of Ni or Pt. Thus, the ligand field calculations for NiAu and AlNi differ only in the value of the bond length. For both molecules a value of $\zeta_{3d}(\mathrm{Ni},3d^9 4s^1) = 603.0\ \mathrm{cm}^{-1}$ was used.[35] The values of $\langle r^2\rangle_{3d} = 0.4246\ \text{Å}^2$ and $\langle r^4\rangle_{3d} = 0.5541\ \text{Å}^4$ were obtained from a Hartree–Fock calculation on the $3d^9 4s^1$, ^3D state of atomic nickel,[36] corrected by the ratio of the relativistic expectation values of $\langle r^2\rangle_{3d}$ and $\langle r^4\rangle_{3d}$ to the nonrelativistic values for the $3d^{10}4s^1$, ^2S ground state of the copper atom.[37] This relativistic correction increased the Hartree–Fock values of $\langle r^2\rangle_{3d}$ and $\langle r^4\rangle_{3d}$ by only 1.26% and 3.19%, respectively, indicating that the error associated with using nonrelativistic Hartree–Fock expectation values is minimal. Correcting by the ratio of the relativistic to the nonrelativistic expectation values for copper probably leads to values of $\langle r^2\rangle_{3d}$ and $\langle r^4\rangle_{3d}$ which are in error by less than 0.5%. The experimentally determined bond lengths of $r_0(\mathrm{AlNi}) = 2.3211(7)$ Å,[30] and $r_0(\mathrm{NiAu}) = 2.351(1)$ Å (Ref. 31) were used in the calculation for AlNi and NiAu, respectively.

The ligand field calculation of the ground manifold of PtCu used $\zeta(\mathrm{Pt},5d^9 6s^1) = 4052.8\ \mathrm{cm}^{-1}$ (obtained from Moore's tables[38] as $2/5[E(5d^9 6s^1, {}^3D_1) - E(5d^9 6s^1, {}^3D_3)]$), $\langle r^2\rangle_{5d} = 0.9211\ \text{Å}^2$,[37] and $\langle r^4\rangle_{5d} = 1.7306\ \text{Å}^4$.[37] These expectation values are taken from a Dirac–Fock relativistic calculation on the platinum atom in its $5d^9 6s^1$, ^3D ground state. Again, the experimental bond length of $r_0(\mathrm{PtCu}) = 2.335(1)$ Å (Ref. 31) was used. Results of the ligand field calculations are presented with the experimental data in Tables I, II, and III below.

III. EXPERIMENT

Dispersed fluorescence (DF) spectroscopy was used to investigate supersonically cooled AlNi, NiAu, and PtCu diatomic molecules. The molecules were formed by pulsed laser ablation (Nd:YAG, 1064 nm) of either an AlNi (1:1), a NiAu (1:1), or a PtCu (1:2) metal alloy disk, followed by supersonic expansion in helium carrier gas (120 psig). The metal target disks were prepared by electric arc furnace melting of equimolar samples of aluminum and nickel for the AlNi (1:1) sample, and of nickel and gold for the NiAu (1:1) sample. The bond energy of Pt_2 (3.14 ± 0.02 eV) (Ref. 39) is much greater than that of Cu_2 (2.03 ± 0.02 eV),[2] and is probably also greater than the bond energy of PtCu. To decrease the probability of collisions between PtCu and Pt atoms, which would be likely to destroy the PtCu molecule via the displacement reaction,

$$\mathrm{Pt} + \mathrm{PtCu} \rightarrow \mathrm{Pt}_2 + \mathrm{Cu}, \tag{3.1}$$

the amount of platinum was decreased in the sample, and the PtCu sample was prepared as a 1:2 molar alloy (Pt:Cu).

From the point of vaporization, the ablated metal atoms were entrained in a pulse of helium carrier gas and traveled through a 5.9 cm long channel, 2 mm in diameter, prior to expansion into vacuum (1×10^{-3} Torr) through a 2 mm orifice. The resulting jet-cooled molecular beam was excited by a Nd:YAG pumped tunable dye laser ($\approx 0.7\ \mathrm{cm}^{-1}$ resolution) which crossed the molecular beam at right angles 1 cm downstream from the exit orifice. The laser radiation entered and exited the chamber through baffled tubes with Brewster angle windows to reduce the scattered radiation in the chamber.

The resulting fluorescence was collected at right angles to both the molecular beam and the excitation radiation. A 3.5 in.diam $\times$ 0.25 in. thick window separated the collection optics from vacuum, such that the optics were optically isolated from the chamber except through the window. A cone, tapering from a 3 in. opening at the window down to a 0.75 in. opening 0.375 in. above the center of the viewing area, painted with flat black paint, was used to reduce stray light entering the collection optics. A simple, 3 in. diam, two-lens system was used to collimate and focus the light into the monochromator, matching the F-number of the monochromator. The fluorescence collected was dispersed using a Spectral Energy GM 252 monochromator (Czerny–Turner-type, 250 mm, f/3.6 aperture ratio, 33 Å/mm dispersion grating with a 500 nm blaze) outfitted with a McPherson 789 A-1 scan drive operated under computer control (IBM PC compatible 386). The dispersed light was detected with a Hamamatsu R3896 photomultiplier tube. The current signal was then amplified and converted to a voltage signal with a home built preamplifier, and sent to a gated integrator (Evans Associates Model 4130) using a gate width of 1 μs. The output of the gated integrator was then digitized and stored for further processing by the computer.

Perhaps due to damage suffered in shipping, the monochromator suffered from an oscillatory deviation from the true wavelength which was as large as 0.5 nm. This error was corrected using calibration data which were collected in 1 nm increments using scattered laser light from the tunable dye laser mentioned above. The resulting calibration curve was interpolated to convert the measured emission wave numbers to true wave numbers. Previous work with this dye laser has shown that it is calibrated to within $\pm 3\ \mathrm{cm}^{-1}$, so the absolute accuracy of band positions reported here is thought to be approximately $\pm 5\ \mathrm{cm}^{-1}$.

In studies of mixed diatomic metals such as AlNi, NiAu, and PtCu, it is obviously impossible to avoid concomitant

production of the homonuclear molecules Al_2 and Ni_2, Ni_2 and Au_2, and Pt_2 and Cu_2, respectively. It is therefore important to verify that the observed fluorescence originates from the desired mixed metal molecule, and not from one of the homonuclear species which are invariably also present. In the case of AlNi, fluorescence originating from Al_2 was not a problem because jet-cooled Al_2 has no absorptions in the region probed here.[40] (The $B\,^3\Sigma_u^- - A\,^3\Sigma_g^-$ system previously observed in a King furnace[41,42] is not observed under jet-cooled conditions, due to lack of population in the $A\,^3\Sigma_g^-$ state.) Likewise, because the states probed in AlNi lay above the Ni_2 predissociation threshold at 16 658 cm^{-1},[25] excitation of Ni_2 in addition to AlNi led to predissociation of the Ni_2, rather than fluorescence, eliminating any possible ambiguity in the carrier of the fluorescence spectrum. In the case of NiAu, the transitions probed also lay above the Ni_2 predissociation threshold, again eliminating interferences due to the Ni_2 molecule. In addition, the spectrum of Au_2 is rather sparse, and it was not difficult to avoid the well-known absorptions of Au_2 when investigating NiAu. In the case of PtCu, it was likewise easy to avoid the well-known absorptions due to Cu_2. A greater difficulty arose, however, because a large quantity of Pt_2 was produced in addition to PtCu. Because Pt_2 has a severely congested spectrum[39] in the region of the PtCu transitions that were excited in this study, a pure platinum sample was tested immediately after the PtCu (1:2) sample, without changing the dye laser wavelength. If no fluorescence was observed with the Pt sample, the experimental conditions were then checked using a Pt_2 transition close in wavelength. This produced a quantity of DF spectra of Pt_2, which have been reported in another paper.[26] All of the DF spectra reported in the present investigation disappeared when the PtCu (1:2) sample was replaced with the pure Pt sample, making us confident that they truly arise from diatomic PtCu.

IV. RESULTS

A. Dispersed fluorescence (DF) spectra of AlNi

1. Excitation of the $\Omega' = 7/2 \leftarrow \Omega'' = 5/2$ transition at 18 076 cm^{-1}

Figure 1 presents DF spectra of AlNi resulting from three different excitations, all of which have been rotationally resolved in a previous resonant two-photon ionization study.[30] Unfortunately, all three excitations occur in an extremely congested part of the AlNi spectrum, and none could be assigned to an identifiable vibronic progression. As a result, upper state vibrational quantum numbers are unknown for all of the excitations.

In the lower panel, a DF spectrum from excitation of an $\Omega' = 7/2 \leftarrow X\,^2\Delta_{5/2}$ band at 18 076 cm^{-1} is displayed. This is plotted as a function of relative wave number, given as the shift from the excitation wave number. The excitation is thought to originate from the $v'' = 0$ level of the ground state, because it was observed as an intense transition in a beam of supersonically cooled molecules. This is confirmed in the DF spectrum by the lack of emission to the blue of the excitation wave number. Similar results apply to the other AlNi bands excited in the present study, allowing it to be concluded that all three excitations originate from the $v'' = 0$ level of the $X\,^2\Delta_{5/2}$ ground state of AlNi.

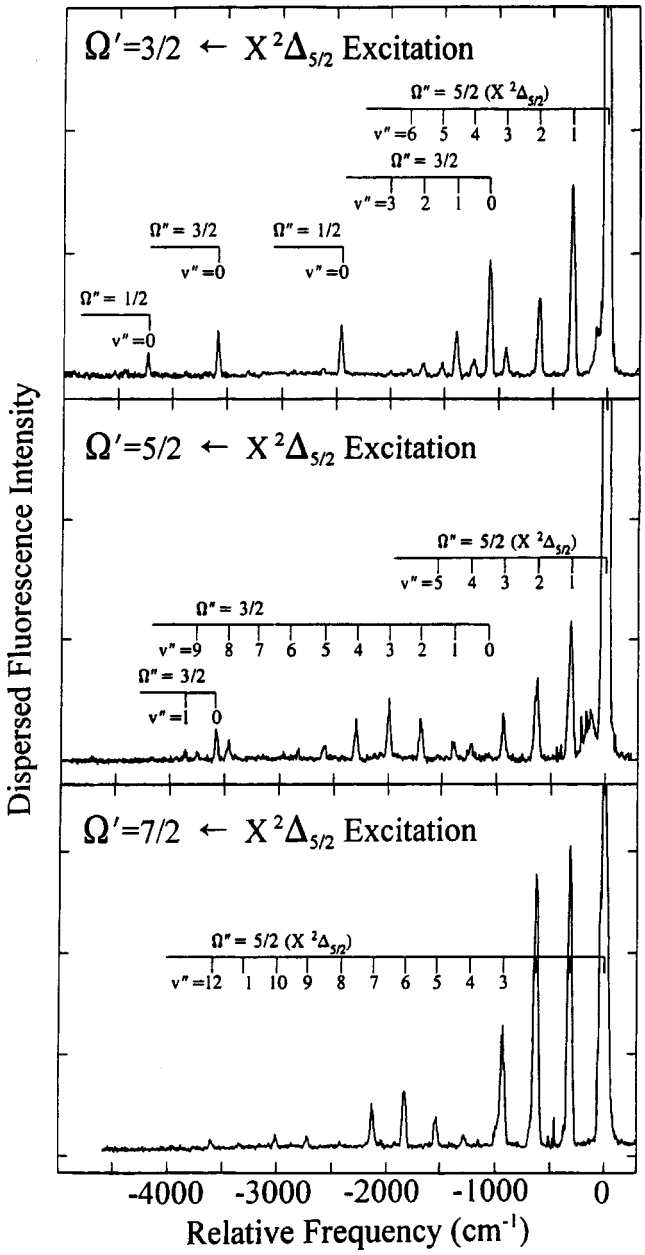

FIG. 1. Dispersed fluorescence spectra resulting from excitation of the AlNi transitions at 18 076 cm^{-1} (bottom panel), 18 265 cm^{-1} (center panel), and 17 762 cm^{-1} (top panel). The spectra have been plotted vs frequency relative to the excitation frequency, so that the corresponding features are aligned.

Excitation of the $\Omega' = 7/2 \leftarrow X\,^2\Delta_{5/2}$ band at 18 076 cm^{-1} results in the observation of a single vibrational progression, terminating in the $X\,^2\Delta_{5/2}$ ground state. Although dipole selection rules would permit the excited $\Omega' = 7/2$ level to fluoresce to levels with $\Omega'' = 9/2$, 7/2, or 5/2, the $3d_{Ni}^9 3s_{Al}^2 \sigma^2$ manifold of states generates only one state corresponding to these possibilities, the $X\,^2\Delta_{5/2}$ ground state. As a result, emission is only observed to the $X\,^2\Delta_{5/2}$ ground state.

The pattern of emission intensity displays obvious nodes near the features corresponding to emission to $v'' = 4$ and

TABLE I. Low-lying states of AlNi.

State	Relative energy (cm^{-1})		Experimental results	
	Ligand field	Experiment	ω_e (cm^{-1})	$\omega_e x_e$ (cm^{-1})
$\Omega=1/2$	3 547	4 210[a]	⋯	⋯
$\Omega=3/2$	2 150	3 570[a]	$\Delta G_{1/2}=279\pm15$[b]	⋯
$\Omega=1/2$	1 905	2 450[a]	⋯	⋯
$\Omega=3/2$	821	1 078[a]	311.4 ± 2.5	1.48 ± 0.24
$X\,^2\Delta_{5/2}$	0	0	314.1 ± 1.1	1.14 ± 0.09

[a]Estimated error is ±5 cm^{-1}. The root-mean-square residual in the vibronic fit is 4.25 cm^{-1}, based on 33 measured fluorescence bands.
[b]Measured from a single weak feature.

$v''=8$, indicating that the upper state is an excited vibrational level of the $\Omega'=7/2$ state, probably corresponding to $v'=2$. This is supported by the isotope shift found in the previous rotationally resolved study, given as $\nu_0(^{27}Al^{58}Ni)-\nu_0(^{27}Al^{60}Ni)=3.6$ cm^{-1}.[30]

Of the molecules investigated here, AlNi provided by far the weakest fluorescence signal. As a result, the apparent intensity of emission at the excitation wavelength is grossly exaggerated; most of the signal at this wavelength is due to scattered laser light, rather than molecular emission. The low intensity of the AlNi emission results from two factors: (1) The excited states have lifetimes in the range of 6–9 μs,[30] and the imaged region of the molecular beam is only 1.8 mm in length. The beam velocity of helium is 1.8 mm/μs, so within 1 μs an excited AlNi molecule will translate out of the viewing area. For states with lifetimes of 6–9 μs, this implies that 85%–90% of the excited molecules translate out of the viewing area before fluorescing. (2) It seems that rather few AlNi molecules were actually produced in the present series of experiments, at least as compared to the numbers of NiAu and PtCu molecules that could be produced. This may have been due to oxygen impurities in either the AlNi sample or the helium carrier gas; these would be expected to be much more reactive with AlNi than with either NiAu or PtCu.

Because emission to the $X\,^2\Delta_{5/2}$ ground state was observed in the DF spectra for all three excitations that were employed, the three spectra were combined to provide a global fit of the vibrational levels of the ground and low-lying states. To perform the fit, the emission band positions were shifted by the excitation wave number so that the resulting wave numbers corresponded directly to the energy of the lower state of the emission. The results of the fit, along with the results of the ligand field calculation described in Sec. II above, are provided in Table I. For AlNi and all of the molecules investigated here, the wave numbers of the fluorescence bands observed, along with the residuals in the vibronic fit, are available via the Electronic Physics Auxiliary Publication Service (EPAPS) or through the author (M.D.M.).[43]

2. Excitation of the $\Omega'=5/2\leftarrow\Omega''=5/2$ transition at 18 265 cm^{-1}

The center panel of Fig. 1 displays the DF spectrum obtained when the 18 265 cm^{-1} $\Omega'=5/2\leftarrow\Omega''=5/2$ transition of AlNi is excited. In addition to a vibrational progression in the ground $X\,^2\Delta_{5/2}$ state, fluorescence to two low-lying states is observed. The symmetry of these low-lying states may be deduced from the selection rule $\Delta\Omega=0,\pm1$. The $X\,^2\Delta_{5/2}$ ground state derives from the $3d^9_{Ni}3s^2_{Al}\sigma^2$ manifold of states, which is expected to provide the most strongly bound states of the molecule. The remaining states which derive from this manifold are characterized by $\Omega=3/2$ (two states) and $\Omega=1/2$ (two states). Allowed emissions from the $\Omega'=5/2$ state at 18 265 cm^{-1} must terminate on levels with $\Omega''=7/2$, 5/2, or 3/2, thereby identifying the two new states as having $\Omega''=3/2$.

These two low-lying states were also observed in the DF spectrum from the $\Omega'=3/2\leftarrow\Omega''=5/2$ excitation at 17 762 cm^{-1}, described in Sec. IV A 3. Therefore a global fit similar to that performed for the ground state was employed for the low-lying $\Omega=3/2$ states. The resulting spectroscopic constants are again listed in Table I. The highest wave number band observed in each progression was assumed to be emission to the $v''=0$ level in the low-lying state, but this is not absolutely certain. This is discussed further in Sec. IV A 3 below. As was the case in the $\Omega'=7/2\leftarrow X\,^2\Delta_{5/2}$ excitation at 18 076 cm^{-1}, the excitation band at 18 265 cm^{-1} could not be assigned as a member of a vibrational progression due to the congestion of the vibronic spectrum. The reported isotope shift of 1.6 cm^{-1} for this excitation suggests that $v''>0$, however.[30]

A surprising feature of this DF spectrum is that the intensity pattern in the vibrational bands terminating on the three lower states varies quite significantly from state to state. A monotonically decreasing pattern of intensities is found for emission to the $X\,^2\Delta_{5/2}$ ground state, with $v''=5$ being the last observed level. In contrast, emission to the lower of the $\Omega''=3/2$ states exhibits a long progression out to $v''=9$, with a node in intensity near $v''=7$. Finally, the emission to the higher energy $\Omega''=3/2$ state displays a very short progression containing only two vibronic bands. Given that all of these states are thought to be derived from the $3d^9_{Ni}3s^2_{Al}\sigma^2$ manifold, they should have similar potentials, differing only in the location of the $3d$ hole on the nickel $3d^9$ core. This expectation is supported by the similarity of the vibrational frequencies obtained for these low-lying states (see Table I). According to the Franck–Condon principle, however, emissions to states with similar potentials should give similar vibronic progressions, unlike what is observed here. Either the emission is not governed by the Franck–Condon principle, or the potentials of the low energy states are not as similar as one might expect.

A likely explanation of this observation, which retains the assumption that the potential curves of the low energy states are similar, invokes the fact that the upper state of this emission lies in a congested region of the AlNi spectrum where coupling to many different electronic states may be significant. Rather than thinking of the upper state as a single Born–Oppenheimer state which may be written as a product of an electronic wave function (ϕ_i) times a vibrational wave function (χ_v), it is probably more appropriate to think of the upper state as a strongly mixed combination of such product wave functions,

$$\Psi(q,R)=\sum_{i,v} C_{i,v}\phi_i(q|R)\chi_v(R). \quad (4.1)$$

With a mixed upper state wave function of the form given in Eq. (4.1), emission to different electronic states may be governed by different electronic-vibrational contributions, possibly resulting in very different Franck–Condon profiles for emission to different electronic states. Thus, different pieces of the mixed wave function (4.1) may be responsible for emission to the various electronic states, causing the vibrational progressions in each emission system to display a different intensity pattern.

Finally, one more observation about the spectrum in the center panel of Fig. 1 is in order. In addition to the intense signal at 0 cm^{-1}, which is primarily due to scattered excitation radiation, a weak, broad feature is evident near a relative wave number of -200 cm^{-1}. This is due to scattered excitation radiation as well, but in this case it is caused by amplified spontaneous emission (ASE) in the dye laser, which was operated on Fluorescein 548. The intensity of the ASE was too weak to excite molecular transitions in AlNi, as may be judged by comparing its intensity to that of the scattered excitation radiation at 0 cm^{-1}.

3. Excitation of the $\Omega'=3/2\leftarrow\Omega''=5/2$ transition at 17 762 cm^{-1}

The upper panel of Fig. 1 displays the DF spectrum resulting from excitation of the AlNi $\Omega'=3/2\leftarrow\Omega''=5/2$ transition at 17 762 cm^{-1}.[30] Fluorescence to the ground $X\,^2\Delta_{5/2}$ state, as well as to both of the low-lying $\Omega=3/2$ states is observed. In addition, two new isolated peaks are observed. These are assigned as the two $\Omega=1/2$ states arising from the ground $3d^9_{\mathrm{Ni}}3s^2_{\mathrm{Al}}\sigma^2$ manifold of states. Thus, the observed emissions correspond to all of the allowed possibilities, $\Omega'=3/2\rightarrow\Omega''=5/2$, $\Omega'=3/2\rightarrow\Omega''=3/2$, and $\Omega'=3/2\rightarrow\Omega''=1/2$.

As for the other excitation bands investigated here, this band was not assigned to a vibronic progression in the original investigation of AlNi, and no upper state vibrational number was provided.[30] Nevertheless, a small isotope shift of 0.3 cm^{-1} was observed, suggesting that the band is vibrationally a 0–0 band. This is consistent with the lack of nodal structure in the intensities of the emissions to the $X\,^2\Delta_{5/2}$ ground state and to the low energy $\Omega''=3/2$ state. On the other hand, assignment of the upper state as having $v'=0$ implies that it is not significantly mixed with other Born–Oppenheimer states in the sense of Eq. (4.1). Given the density of vibronic states in the published spectrum of AlNi,[30] it seems unlikely that such nonadiabatic mixing could be avoided.

Although fluorescence to all five states arising from the $3d^9_{\mathrm{Ni}}3s^2_{\mathrm{Al}}\sigma^2$ manifold of AlNi has now been observed and assigned by Ω-value, it is difficult to assign a vibrational numbering for the levels of the $\Omega=1/2$ states with certainty. In these states only a single vibrational level has been observed. Our efforts to expand this study by excitation of other vibronic features in the spectrum of AlNi have met with no success, owing to the weak fluorescence signal found for this molecule. In the absence of evidence to the contrary, the single bands found for the $\Omega=1/2$ states are assigned as fluorescence to $v''=0$ levels. Consequences of a possible misassignment are considered in Sec. V A below.

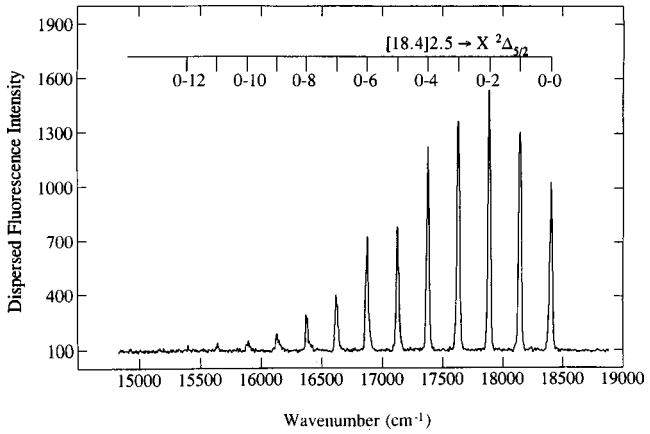

FIG. 2. Dispersed fluorescence spectrum resulting from excitation of the 0–0 band of the $[18.4]2.5\leftarrow X\,^2\Delta_{5/2}$ system of NiAu.

B. Dispersed fluorescence (DF) spectra of NiAu

1. Excitation of the 0–0, 1–0, 3–0, 4–0, and 5–0 bands of the $[18.4]2.5\leftarrow X\,^2\Delta_{5/2}$ system

The DF spectra resulting from excitation of the 0–0 and 1–0 bands of the $[18.4]2.5\leftarrow X\,^2\Delta_{5/2}$ system[31] of NiAu are displayed in Figs. 2 and 3, respectively. The $v'=0$ level of the [18.4]2.5 state has a measured lifetime of 6.2 μs, which is quite comparable to that found for the excited states of AlNi. Nevertheless, the DF signal obtained for NiAu was much more intense than that found for AlNi, allowing the monochromator slits to be narrowed to provide much better resolution. In addition, a realistic fluorescence intensity at the excitation wave number is obtained, because the signal level is much higher than the scattered light signal. A stronger than expected signal was also observed in the previous R2PI study,[31] indicating efficient production of NiAu in the molecular beam.

As may be seen in Fig. 2, the fluorescence resulting from excitation of the 0–0 band forms a single progression termi-

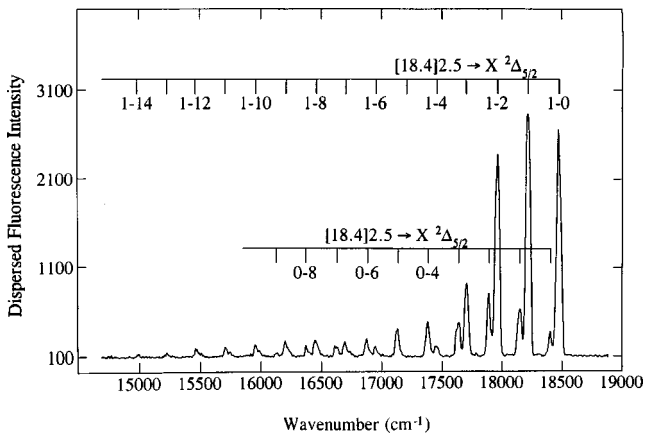

FIG. 3. Dispersed fluorescence spectrum resulting from excitation of the 1–0 band of the $[18.4]2.5\leftarrow X\,^2\Delta_{5/2}$ system of NiAu.

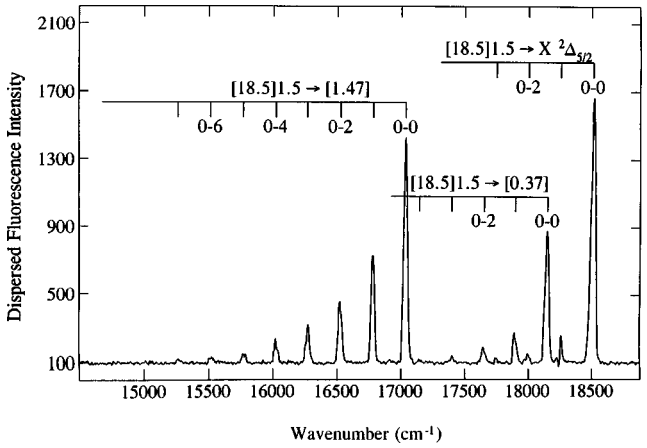

FIG. 4. Dispersed fluorescence spectrum resulting from excitation of the 0–0 band of the $[18.5]1.5 \leftarrow X\,^2\Delta_{5/2}$ system of NiAu.

nating in the ground electronic state. Unfortunately, no fluorescence to low-lying excited states was observed. In contrast, the DF spectrum resulting from excitation of the 1–0 band, displayed in Fig. 3, appears more complicated. In addition to the vibrational progression from the excited $v'=1$ level to the ground electronic state, another vibrational progression appears at the same wave numbers and showing the same intensity pattern as the fluorescence from the $v'=0$ level to the ground electronic state. Although not displayed in this paper, the DF spectra of the 3–0, 4–0, and 5–0 excitations are even more complicated. For each of these excitations, fluorescence was observed as a progression from the excited vibrational level to the ground state, along with fluorescence from lower vibrational levels to the ground state. Evidently, collisions with helium carrier gas cause vibrational relaxation within the [18.4]2.5 state of NiAu to occur on a time scale comparable to that of fluorescence, so that partially relaxed fluorescence is observed.

None of the other molecules investigated in this study have exhibited vibrationally relaxed fluorescence, despite the fact that all have been probed at the same point, 1 cm downstream from the 2 mm expansion orifice, and despite the similarity in fluorescence lifetimes in all three molecules. A likely explanation for the rapid collisional relaxation of excited vibrational levels of the [18.4]2.5 state of NiAu may be found by noting that this excited state has a vibrational frequency of 79.45 ± 1.03 cm^{-1},[31] which is unusually small for a transition metal diatomic molecule. Although the vibrational frequencies of the excited states of AlNi and PtCu which were probed in the present study are not known, they are likely much greater than the frequency of the [18.4]2.5 state of NiAu. The low collision energies available in the excitation region are expected to favor quenching of low frequency vibrations, offering an explanation of why collisional vibrational quenching was only observed for NiAu.

2. Excitation of the 0–0 band of the $[18.5]1.5 \leftarrow X\,^2\Delta_{5/2}$ system

Figure 4 displays the DF spectrum resulting from excitation of the 0–0 band of the $[18.5]1.5 \leftarrow X\,^2\Delta_{5/2}$ system. In addition to the fluorescence terminating in the ground electronic state, fluorescence to two low-lying states is also observed. Unfortunately, fluorescence to neither of these states was observed from the [18.4]2.5 state, so the Ω-values of these states cannot be assigned with certainty. Presumably these states correspond to two of the remaining four states [$\Omega = 3/2$ (two states) and $\Omega = 1/2$ (two states)] derived from the $3d^9_{\mathrm{Ni}}5d\sigma^2$ manifold. Each of these progressions was fitted to extract spectroscopic constants. The resulting fitted constants, along with those of the ground state, are given in Table II along with the results of the ligand field calculation.

C. Dispersed fluorescence (DF) spectra of PtCu

In the previous resonant two-photon ionization study of PtCu, two band systems were assigned,[31] with rotationally resolved studies successfully providing an Ω-value assignment for the $[19.6]1.5 \leftarrow X\,^2\Delta_{5/2}$ system. In the present investigation, attempts to excite this system and obtain DF data were not successful, primarily due to excitation of other bands of PtCu and Pt_2 by amplified spontaneous emission of the dye laser in this wave number range. However, excitation of eight previously unpublished bands, having lifetimes ranging from 1.6 to 4.8 μs, was successful.

Figure 5 displays the DF spectrum resulting from excitation of the PtCu transition at 17 266 cm^{-1}. In all of the PtCu transitions studied, fluorescence to low vibrational levels was strongly favored, implying small changes in bond length upon electronic excitation and emission. As was found for NiAu, the fluorescence signal at the excitation wave number was much greater than the scattered light intensity.

TABLE II. Low-lying states of NiAu.

Ligand field		Experimental results			
State	Energy (cm^{-1})	State	Energy (cm^{-1})	ω_e (cm^{-1})	$\omega_e x_e$ (cm^{-1})
$\Omega = 1/2$	3 462	⋯	⋯	⋯	⋯
$\Omega = 3/2$	2 115	⋯	⋯	⋯	⋯
$\Omega = 1/2$	1 841	[1.47]0.5[a]	1 475[b]	258.4 ± 1.6	0.88 ± 0.16
$\Omega = 3/2$	806	[0.37]1.5[a]	368[b]	250.5 ± 1.5	0.45 ± 0.24
$X\,^2\Delta_{5/2}$	0	$X\,^2\Delta_{5/2}$	0	259.4 ± 0.4	0.72 ± 0.03

[a]For this state the Ω-value is not experimentally known, but is tentatively identified on the basis of comparison to the ligand field model.

[b]Estimated error is ±5 cm^{-1}. The root-mean-square residual in the vibronic fit is 3.27 cm^{-1}, based on 96 measured fluorescence bands.

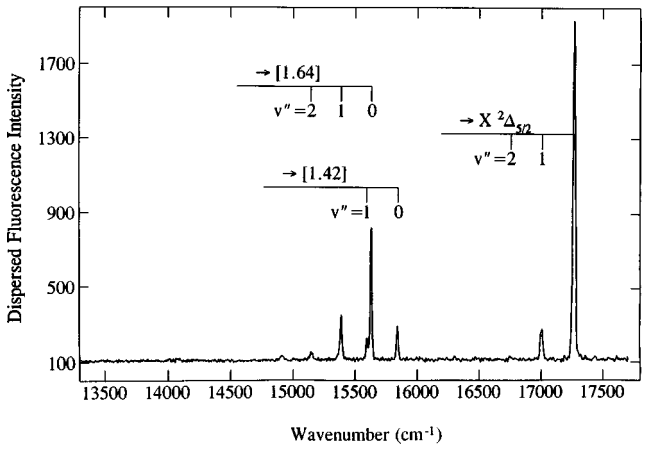

FIG. 5. Dispersed fluorescence spectrum resulting from excitation of PtCu at 17 266 cm^{-1}.

In addition to the very short vibrational progression found for emission to the $X\,^2\Delta_{5/2}$ ground state, two low-lying electronic states were observed, as shown in Fig. 5. These states, labeled the [1.42] and [1.64] states, were found to be separated by very nearly a vibrational quantum of the [1.42] state, so that the [1.42] $v=1$ and [1.64] $v=0$ levels fell at nearly the same energy. To resolve these features a slit width of 0.10 mm was required, giving a resolution of approximately 20 cm^{-1} FWHM. To resolve the fluorescence to these two low-lying states and to obtain accurate band positions for the strong fluorescence features, each DF spectrum was recorded with narrow slits (0.10 mm). To obtain wave numbers for the weaker features in the DF spectrum, a second dispersed fluorescence scan was performed with wider slits (0.35 mm).

The data from each of the excitations were shifted by the excitation wave number to obtain the energy of the lower level. All of the fluorescence data terminating in the ground state could be combined into a single fit to obtain spectroscopic constants. The data for each of the two low-lying states were fitted in a similar manner. Final spectroscopic constants are listed in Table III along with the results of the ligand field calculation described in Sec. II.

The ground state vibrational constants obtained in the present study of PtCu (which give $\Delta G_{1/2}=255.2\pm3.6\ cm^{-1}$) are in disagreement with the value $\Delta G_{1/2}=288.20\pm1.66\ cm^{-1}$ reported in the previous R2PI study of this molecule.[31] This previous value was determined from the wave numbers of three bands that were thought to be hot bands of the $[17.6]\leftarrow X\,^2\Delta_{5/2}$ system. The residuals for the fit of these three putative hot bands, 3.78, 0.29, and −4.06 cm^{-1} for the 2–1, 3–1, and 4–1 bands, respectively, were much larger than the average magnitude of the residuals for the fit of this band system (0.79 cm^{-1} for the nine other bands in the fit). In addition, the errors in this fit show a systematic trend that is suspicious in retrospect. It is now clear, given the large number of bands excited in the present study and the quality of the vibrational fit, that the previously reported value of $\Delta G_{1/2}$ was incorrect, and that the three bands previously assigned as hot bands actually formed an entirely different electronic band system.

V. DISCUSSION

Of the three molecules studied, AlNi and NiAu are expected to be best described by the ligand field model. This is because the $3d$ orbitals of nickel are the most compact of any of the open d subshell transition metals, and are much smaller than the $5d$ orbitals of platinum. Thus, the approximation required by the model that the d orbitals do not overlap to form bonding and antibonding combinations is expected to be most valid in the case of the nickel-containing metal molecules. In addition, it is in the examples of NiCu and Ni_2 that the ligand field model has had its greatest success, through its comparisons to the results of *ab initio* quantum chemistry.[28]

A. AlNi: Comparison between experimental and ligand field results

The results of the ligand field calculation described in Sec. II for AlNi are listed in Table II, along with the experimentally determined energies for the ground $3d^9_{Ni}3s^2_{Al}\sigma^2$ manifold of states. While the results are not in quantitative agreement, the ligand field model does correctly predict the ordering of the states belonging to the $3d^9_{Ni}3s^2_{Al}\sigma^2$ manifold.

In comparisons of ligand field results to experiment, it has frequently been necessary to allow the ligand field parameters to vary in order to reproduce experimental data. The net result is a fit of several electronic states subject to some constraints, such as constancy of the spin–orbit parameter, ζ, for example. When properly implemented this approach leads to a smaller number of spectroscopic parameters than are required when more conventional fitting procedures are employed. More importantly, the reduced number of spectro-

TABLE III. Low-lying states of PtCu.

Ligand field		Experimental results			
State	Energy (cm^{-1})	State	Energy (cm^{-1})	ω_e (cm^{-1})	$\omega_e x_e$ (cm^{-1})
$\Omega=1/2$	14 239	⋯	⋯	⋯	⋯
$\Omega=3/2$	10 873	⋯	⋯	⋯	⋯
$\Omega=1/2$	4 296	[1.64][a]	1 638[b]	241.6±2.6	0.68±0.67
$\Omega=3/2$	2 171	[1.42][a]	1 424[b]	241.5±6.7	−0.10±2.27
$X\,^2\Delta_{5/2}$	0	$X\,^2\Delta_{5/2}$	0	258.6±3.1	1.69±0.82

[a]The Ω-value of this state is not experimentally known.

[b]Estimated errors in the energy of the low-lying states are ±5 cm^{-1}. The root-mean-square residual in the vibronic fit is 3.03 cm^{-1}, based on 42 measured fluorescence bands.

scopic parameters that are obtained are physically meaningful and may be used to predict the energy of states which have not yet been observed.

In an attempt to understand the observed states of AlNi in the context of the ligand field model, we have performed a fit of the ligand field Hamiltonian to the observed states, allowing the effective charge of the ligand, Z_{Al}, and the spin–orbit parameter, ζ, to vary. The resulting fit was poor, with errors in the range of several hundred cm^{-1}. Although the ligand charge converged to a reasonable value of $Z_{Al}=+0.96$, the spin–orbit parameter converged to an unphysically large value of $\zeta=989\ cm^{-1}$. This differs so significantly from the atomic value of $\zeta_{3d}(Ni,3d^9 4s^1)=603.0\ cm^{-1}$ as to invalidate any physical meaning which might be attached to the fit.

A second attempt to fit a model Hamiltonian to the data employed a matrix Hamiltonian with term energies (T_Σ, T_Π, and T_Δ) for the Hund's case (a) basis set, to which the spin–orbit Hamiltonian matrix was added. Again, only a poor result was obtained, and the fitted value of ζ was unphysically large. Finally, a procedure similar to that employed by Gray *et al.* in fitting the levels of the $3d^9_{Ni}\sigma^2$ manifold of NiH,[33] was used. In the NiH study it was recognized that configurational mixing between the $^2\Sigma^+$ state deriving from the $3d^9_{Ni}\sigma^2$ manifold and the $3d^{10}_{Ni}\sigma^1$, $^2\Sigma^+$ state could occur, with the result that the off-diagonal spin–orbit matrix elements connecting the $^2\Sigma^+$ and $^2\Pi_{1/2}$ states in Eq. (2.4) are reduced. The analogous situation was mimicked in AlNi by using a matrix Hamiltonian with term energies (T_Σ, T_Π, and T_Δ) on the diagonal, to which the spin–orbit Hamiltonian is added. To include the effect of configurational mixing between the two $^2\Sigma^+$ states, the off-diagonal spin–orbit matrix element connecting the $^2\Sigma^+$ and $^2\Pi_{1/2}$ states was reduced by multiplication by a constant, c. The parameters T_Σ, T_Π, T_Δ, ζ, and c were then adjusted to fit the measured levels. Because there were an equal number of parameters to be determined and experimental energy levels to be used as input, the concept of "fit" does not apply. Despite the generality of this model Hamiltonian, a very unrealistic value of $\zeta=997\ cm^{-1}$ was obtained. This indicates problems in either the model or the experimental data.

Given the results of these attempts, and the fact that the energies of the two $\Omega=1/2$ states are based on a single fluorescence band, the only definite conclusion that may be drawn is that the ligand field model correctly predicts the ordering of the $3d^9_{Ni}3s^2_{Al}\sigma^2$ manifold of states. A graphical comparison of the experimental values and the ligand field results (obtained without varying any parameters) is provided in Fig. 6. In considering the comparison of ligand field theory and experiment provided by this figure, it is useful to keep in mind that the vibrational assignments of the three highest lying states are not certain, so the reported energies for these states should be considered upper limits rather than exact values.

B. NiAu: Comparison between experimental and ligand field results

The results of the ligand field calculation described in Sec. II of this article, as well as the experimentally determined energies for two of the states in the ground $3d^9_{Ni}5d^{10}_{Au}\sigma^2$ manifold of states of NiAu and two of the states in the ground $5d^9_{Pt}3d^{10}_{Cu}\sigma^2$ manifold of states of PtCu are listed in Tables II and III, respectively. Unlike the dispersed fluorescence studies of AlNi, the Ω-values of the low-lying states for these molecules could not be assigned. Greater signal levels, however, allowed a more confident assignment of the $v''=0$ levels of the low-lying excited states in the fluorescence spectra.

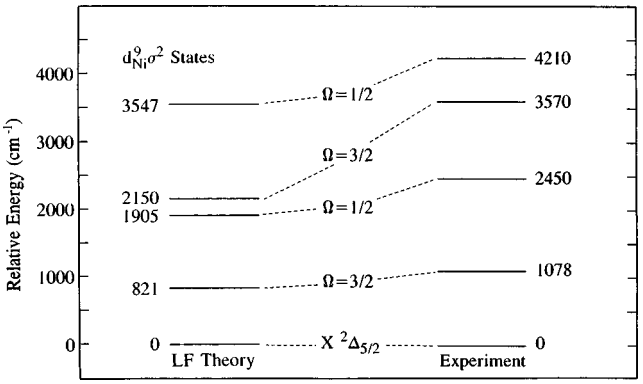

FIG. 6. Comparison of the ligand field energies for the $3d^9_{Ni}3s^2_{Al}\sigma^2$ manifold of states of AlNi with the experimentally determined energies.

One possible cause of failure for the ligand field model would be if the d orbitals were participating in chemical bonding. Relativistic effects in both Pt and Au make the possibility of d orbital contributions to the bonding in these molecules much more probable than in a molecule such as NiCu or Ni_2. Previous resonant two-photon ionization studies of NiAu and PtCu suggest, however, that any d orbital contributions to the bonding in these molecules are very minor.

In the previous spectroscopic study of NiAu and PtCu,[31] the symmetries of the ground states were unambiguously assigned as $^2\Delta_{5/2}$, with the ground state bond lengths determined. The $^2\Delta_{5/2}$ symmetry of the ground states of these molecules results from placement of the hole in a $d\delta$ orbital. This is in contradiction to what one would expect if the d orbital ordering were based on bonding considerations, which would lead to a d-based orbital ordering of $d\sigma<d\pi<d\delta<d\delta^*<d\pi^*<d\sigma^*$ and placement of the d hole in the $d\sigma^*$ orbital, resulting in a $^2\Sigma^+$ ground state. Likewise, a comparison of the bond lengths of NiAu, PtCu, and the filled d orbital counterpart CuAu,[44] which all fall in the range of 2.34 ± 0.01 Å, also supports the conclusion that $d-d$ bonding is negligible in these species. In the present study, the ground state vibrational frequency is determined to be $\omega_e=259\ cm^{-1}$ for both NiAu and PtCu, which is very similar to the ground state vibrational frequency of CuAu, $\Delta G_{1/2}=248\ cm^{-1}$.[44] Again, this supports the conclusion that d orbital contributions to the bonding are minimal in the ground states of NiAu and PtCu.

The two low-lying excited states of NiAu which were located in the present investigation were found 368 and 1475 cm^{-1} above the ground state. Of the levels predicted by the ligand field model, these lie closest to the $\Omega=3/2$ state calculated at 806 cm^{-1} and the $\Omega=1/2$ state calculated at 1841

cm^{-1}, respectively. This suggests, but does not prove, an assignment of the states as the [0.37]1.5 and [1.47]0.5 states, respectively. Without a definite experimental assignment of the Ω values of these states and a determination of the energy of the remaining $\Omega = 3/2$ and 1/2 states, however, a full comparison to the ligand field model is impossible.

C. PtCu: Comparison to the ligand field model and to PtH

The low energy excited states found for PtCu at 1424 and 1638 cm^{-1} are in poor agreement with the results of the simple ligand field plus spin–orbit model, which predicts states at 2171 cm^{-1} ($\Omega = 3/2$) and 4296 cm^{-1} ($\Omega = 1/2$). These two states, along with the $^2\Delta_{5/2}$ ground state, all derive from the splitting of the platinum $5d^9_{Pt}$, $^2D_{5/2}$ core in the axial field of the molecule. The remaining states derived from the PtCu $5d^9_{Pt}3d^{10}_{Cu}\sigma^2$ manifold are derived from the much higher energy $5d^9_{Pt}$, $^2D_{3/2}$ coupling of the electronic spin and orbital angular momenta, and are calculated in the ligand field model to lie at 10 873 cm^{-1} ($\Omega = 3/2$) and 14 239 cm^{-1} ($\Omega = 1/2$). Regardless of the validity of the ligand field model, the large spin–orbit constant of platinum dictates that the electronic states will break up into a low energy set ($\Omega = 5/2$, 3/2, and 1/2) corresponding to the $5d^9_{Pt}$, $^2D_{5/2}$ angular momentum coupling and a much higher energy set ($\Omega = 3/2$ and 1/2), corresponding to the $5d^9_{Pt}$, $^2D_{3/2}$ angular momentum coupling. Thus the two observed states at 1424 and 1638 cm^{-1} are expected to correspond to an $\Omega = 3/2$ and an $\Omega = 1/2$ state. It is impossible to guess which state is which.

In addition to the large spin–orbit interaction in platinum, another fundamental difference between platinum and nickel is the low energy of the $5d^{10}$, ^1S state in platinum as compared to the analogous $3d^{10}$, ^1S state of nickel. After removal of the spin–orbit splitting in the d^9s^1, ^3D term, the energy difference between the d^9s^1, ^3D and $d^{10}s^0$, ^1S states in the two atoms is given as $E(d^{10}, {}^1S) - E(d^9s^1, {}^3D) = 13\,921$ cm^{-1} for nickel and 2087 cm^{-1} for platinum. The much lower energy of the d^{10}, ^1S state in platinum as compared to nickel is expected to lead to a stronger configuration interaction between the $5d^9_{Pt}3d^{10}_{Cu}\sigma^2$, $^2\Sigma^+$ and $5d^{10}_{Pt}3d^{10}_{Cu}\sigma^1$, $^2\Sigma^+$ states than occurs in the analogous $3d^9_{Ni}5d^{10}_{Au}\sigma^2$, $^2\Sigma^+$ and $3d^{10}_{Ni}5d^{10}_{Au}\sigma^1$, $^2\Sigma^+$ states of NiAu. Such an interaction will stabilize the low-lying $\Omega = 1/2$ state of PtCu that derives from the $5d^9_{Pt}$, $^2D_{5/2}$ angular momentum coupling, and may account for the observation of the $^2D_{5/2}$ $\Omega = 3/2$ and 1/2 states at comparable energies.

To our knowledge, no *ab initio* theoretical studies have been performed on PtCu, but the isovalent species, PtH, has been studied by both *ab initio*[45–55] and experimental methods.[34,56–61] In PtH, the large energy separation expected between the $5d^9_{Pt}(^2D_{5/2})\sigma^2$, $\Omega = 5/2$, 3/2, and 1/2 set of states and the $5d^9_{Pt}(^2D_{3/2})\sigma^2$, $\Omega = 3/2$ and 1/2 set of states has been confirmed for the two $\Omega = 3/2$ states, which are found to lie 3 225 and 11 582 cm^{-1} above the $v = 0$ level of the $X\,^2\Delta_{5/2}$ ground state.[34] In addition, the strong configurational mixing expected between the $5d^9_{Pt}3d^{10}_{Cu}\sigma^2$, $^2\Sigma^+$ and $5d^{10}_{Pt}3d^{10}_{Cu}\sigma^1$, $^2\Sigma^+$ states of PtCu has been calculated to occur in the analogous $5d^9_{Pt}\sigma^2$, $^2\Sigma^+$ and $5d^{10}_{Pt}\sigma^1$, $^2\Sigma^+$ states of PtH, greatly stabilizing the low energy $\Omega = 1/2$ states.[50] In the calculations on PtH this effect is so pronounced that the lower states correlating to the $5d^9_{Pt}(^2D_{5/2})\sigma^2$ limit are calculated to fall in the order $X\,^2\Delta_{5/2} < \Omega = 1/2 < \Omega = 3/2$, with the $\Omega = 3/2$ and $\Omega = 1/2$ states reversed in energy as compared to the predictions of the simple ligand field model.[50]

VI. SUMMARY

Dispersed fluorescence spectra have been collected for the bimetallic transition metal diatomics AlNi, NiAu, and PtCu, allowing the measurement of ground state vibrational frequencies and the location of low-lying electronic states in the $d^9\sigma^2$ ground manifold of states for these species. For AlNi, fluorescence to all five of the states derived from this manifold has been observed, and it has been possible to use selection rules to unambiguously assign Ω quantum numbers to the $3d^9_{Ni}3s^2_{Al}\sigma^2$ states. Three of the states were only observed by fluorescence to a single vibrational level, however, and for this reason the $v = 0$ term energies of these states are somewhat in doubt. For NiAu and PtCu, fluorescence to the ground and two low-lying excited states has been observed, but it has not been possible to establish the Ω-values of the two low-energy states with certainty.

Comparisons to a simple ligand-field plus spin–orbit model have been made for all three molecules. For AlNi, the model predicts the energy ordering of the states deriving from the $3d^9_{Ni}3s^2_{Al}\sigma^2$ manifold correctly, but underestimates the magnitude of the splitting between these states. For NiAu, the model predicts $\Omega = 3/2$ and 1/2 states at 806 and 1841 cm^{-1}, respectively, while the observed states fall at 368 and 1475 cm^{-1}. This comparison allows a tentative identification of the Ω-values of these two states as 3/2 and 1/2, respectively. For PtCu the ligand field model predicts $\Omega = 3/2$ and 1/2 states at 2171 and 4296 cm^{-1}, respectively, while the experiments have located states at 1424 and 1638 cm^{-1}. From this result it appears that a substantial configuration interaction is occurring between the $^2\Sigma^+$ states corresponding to the $5d^9_{Pt}3d^{10}_{Cu}\sigma^2$ and $5d^{10}_{Pt}3d^{10}_{Cu}\sigma^1$ electronic configurations, greatly stabilizing the $\Omega = 1/2$ states. This is quite analogous to *ab initio* predictions for the isovalent PtH molecule.

ACKNOWLEDGMENTS

This material is based upon work supported by the National Science Foundation under Grant No. 0078993. We are also indebted to ASARCO Technical Services Center, Salt Lake City, Utah for the loan of 12 g of platinum, as well as for assistance in flattening the sample after arc-melting.

[1] M. D. Morse, Chem. Rev. **86**, 1049 (1986).
[2] M. D. Morse, in *Adv. Metal Semicond. Clusters*, edited by M. A. Duncan (JAI, Greenwich, 1993), Vol. 1, pp. 83–121.
[3] L. M. Russon, S. A. Heidecke, M. K. Birke, J. Conceicao, P. B. Armentrout, and M. D. Morse, Chem. Phys. Lett. **204**, 235 (1993).
[4] L. M. Russon, S. A. Heidecke, M. K. Birke, J. Conceicao, M. D. Morse, and P. B. Armentrout, J. Chem. Phys. **100**, 4747 (1994).
[5] Z. Fu, L. M. Russon, M. D. Morse, and P. B. Armentrout, Int. J. Mass. Spectrom. **204**, 143 (2001).

[6] R. L. Asher, D. Bellert, T. Buthelezi, and P. J. Brucat, Chem. Phys. Lett. **224**, 525 (1994).
[7] R. L. Asher, D. Bellert, T. Buthelezi, and P. J. Brucat, Chem. Phys. Lett. **224**, 529 (1994).
[8] D. Bellert, T. Buthelezi, V. Lewis, K. Dezfulian, D. Reed, T. Hayes, and P. J. Brucat, Chem. Phys. Lett. **256**, 555 (1996).
[9] A. M. James, P. Kowalczyk, R. Fournier, and B. Simard, J. Chem. Phys. **99**, 8504 (1993).
[10] A. M. James, P. Kowalczyk, and B. Simard, Chem. Phys. Lett. **216**, 512 (1993).
[11] J. R. Lombardi and B. Davis, Chem. Rev. **102**, 2431 (2002).
[12] D. G. Leopold and W. C. Lineberger, J. Chem. Phys. **85**, 51 (1986).
[13] D. G. Leopold, J. Ho, and W. C. Lineberger, J. Chem. Phys. **86**, 1715 (1987).
[14] S. M. Casey and D. G. Leopold, J. Phys. Chem. **97**, 816 (1993).
[15] J. Ho, K. M. Ervin, and W. C. Lineberger, J. Chem. Phys. **93**, 6987 (1990).
[16] J. Ho, K. M. Ervin, M. L. Polak, M. K. Gilles, and W. C. Lineberger, J. Chem. Phys. **95**, 4845 (1991).
[17] J. Ho, M. L. Polak, K. M. Ervin, and W. C. Lineberger, J. Chem. Phys. **99**, 8542 (1993).
[18] S. J. Dixon-Warren, R. F. Gunion, and W. C. Lineberger, J. Chem. Phys. **104**, 4902 (1996).
[19] H. Wu, S. R. Desai, and L.-S. Wang, Phys. Rev. Lett. **76**, 212 (1996).
[20] H. Wu, S. R. Desai, and L.-S. Wang, Phys. Rev. Lett. **77**, 2436 (1996).
[21] B. Simard and P. A. Hackett, J. Mol. Spectrosc. **142**, 340 (1990).
[22] B. Simard, P. A. Hackett, A. M. James, and P. R. R. Langridge-Smith, Chem. Phys. Lett. **186**, 415 (1991).
[23] R. S. Ram, C. N. Jarman, and P. F. Bernath, J. Mol. Spectrosc. **156**, 468 (1992).
[24] A. M. James, P. Kowalczyk, B. Simard, J. C. Pinegar, and M. D. Morse, J. Mol. Spectrosc. **168**, 248 (1994).
[25] J. C. Pinegar, J. D. Langenberg, C. A. Arrington, E. M. Spain, and M. D. Morse, J. Chem. Phys. **102**, 666 (1995).
[26] J. C. Fabbi, J. D. Langenberg, Q. D. Costello, M. D. Morse, and L. Karlsson, J. Chem. Phys. **115**, 7543 (2001).
[27] M. B. Airola and M. D. Morse, J. Chem. Phys. **116**, 1313 (2002).
[28] E. M. Spain and M. D. Morse, J. Chem. Phys. **97**, 4641 (1992).
[29] E. M. Spain and M. D. Morse, J. Chem. Phys. **97**, 4633 (1992).
[30] J. M. Behm, C. A. Arrington, and M. D. Morse, J. Chem. Phys. **99**, 6409 (1993).
[31] E. M. Spain and M. D. Morse, J. Chem. Phys. **97**, 4605 (1992).
[32] S. A. Kadavathu, R. Scullman, J. A. Gray, M. Li, and R. W. Field, J. Mol. Spectrosc. **140**, 126 (1990).
[33] J. A. Gray, M. Li, T. Nelis, and R. W. Field, J. Chem. Phys. **95**, 7164 (1991).
[34] M. C. McCarthy, R. W. Field, R. Engleman, Jr., and P. F. Bernath, J. Mol. Spectrosc. **158**, 208 (1993).
[35] J. Sugar and C. Corliss, J. Phys. Chem. Ref. Data Suppl. **14**, 1 (1985).
[36] C. F. Fischer, *The Hartree–Fock Method for Atoms* (Wiley, New York, 1977).
[37] J. P. Desclaux, At. Data Nucl. Data Tables **12**, 311 (1973).
[38] C. E. Moore, *Atomic Energy Levels*, Natl. Bur. Stand. U.S. Circ. No. 467 (U.S. Government Printing Office, Washington, DC, 1971).
[39] S. Taylor, G. W. Lemire, Y. M. Hamrick, Z. Fu, and M. D. Morse, J. Chem. Phys. **89**, 5517 (1988).
[40] Z. Fu, G. W. Lemire, G. A. Bishea, and M. D. Morse, J. Chem. Phys. **93**, 8420 (1990).
[41] P. B. Zeeman, Can. J. Phys. **32**, 9 (1954).
[42] D. S. Ginter, M. L. Ginter, and K. K. Innes, Astrophys. J. **139**, 365 (1963).
[43] See EPAPS Document No. E-JCPSA6-118-001320 for 6 pages of band positions and vibronic fits. A direct link to this document may be found in the online article's HTML reference section. The document may also be reached via the EPAPS homepage (http://www.aip.org/pubservs/epaps.html) or from ftp.aip.org in the directory /epaps/. See the EPAPS homepage for more information.
[44] G. A. Bishea, J. C. Pinegar, and M. D. Morse, J. Chem. Phys. **95**, 5630 (1991).
[45] H. Basch and S. Topiol, J. Chem. Phys. **71**, 802 (1979).
[46] S. W. Wang and K. S. Pitzer, J. Chem. Phys. **79**, 3851 (1983).
[47] A. Gavezzotti, G. F. Tantardini, and M. Simonetta, Chem. Phys. Lett. **129**, 577 (1986).
[48] C. M. Rohlfing, P. J. Hay, and R. L. Martin, J. Chem. Phys. **85**, 1447 (1986).
[49] S. Tobisch and G. Rasch, Chem. Phys. Lett. **166**, 311 (1990).
[50] K. Balasubramanian and P. Y. Feng, J. Chem. Phys. **92**, 541 (1990).
[51] O. Gropen, J. Almlof, and U. Wahlgren, J. Chem. Phys. **96**, 8363 (1992).
[52] L. Visscher, T. Saue, W. C. Nieuwpoort, K. Faegri, and O. Gropen, J. Chem. Phys. **99**, 6704 (1993).
[53] K. G. Dyall, J. Chem. Phys. **98**, 9678 (1993).
[54] T. Fleig and C. M. Marian, Chem. Phys. Lett. **222**, 267 (1994).
[55] T. Fleig and C. M. Marian, J. Chem. Phys. **108**, 3517 (1998).
[56] H. Neuhaus and R. Scullman, Z. Naturforsch. A **19a**, 659 (1964).
[57] R. Scullman, Ark. Fys. **28**, 255 (1964).
[58] B. Kaving and R. Scullman, Can. J. Phys. **49**, 2264 (1971).
[59] B. Kaving and R. Scullman, Phys. Scr. **9**, 33 (1974).
[60] R. Scullman and P. Cederbalk, J. Phys. B **10**, 3659 (1977).
[61] G. Gustafsson and R. Scullman, Mol. Phys. **67**, 981 (1989).